On the Measurement of Nano-Hardness and Elastic Modulus of Ultra-Thin Overcoats: Effect of W-doping and Annealing on the Properties of DLC

Roger Yu Lo and David B. Bogy
Computer Mechanics Laboratory
Department of Mechanical Engineering
University of California, Berkeley
Berkeley, CA 94720

ABSTRACT

The working principal and the methods of analysis for measuring hardness and reduced elastic modulus by a recently commercialized tester are described. The advantage of this approach as compared to techniques based on scanning probe microscopes is discussed. The method of identifying the overcoat thin film modulus from the measured composite value of the film/substrate system is presented. In addition, the method of measuring modulii for non-uniform films is also examined. Nano-indentation tests on bulk fused Quartz with this method show no indentation depth effect. Nano-indentation tests on W-doped diamondlike films (WCx) show that the hardness of these films decreases as the W concentration and the magnitude of the negative substrate bias increase. Comparing the hardness and modulii of annealed and un-annealed DLC films, we found that annealing up to 900°C at temperatures had little influence on the films' mechanical properties.

1. INTRODUCTION

The demand of higher areal density in magnetic storage devices has pushed the protective layers on the disks and sliders, fabricated by a variety of deposition techniques, to extremely small thicknesses. In current products, they vary from 5 to 20 nm. To evaluate the mechanical properties of these ultra thin films, Lu and Bogy[1] employed a scanning probe microscope (SPM), also called a Point Contact Microscope (PCM), originally designed by Kaneko *et al*[2], to study various films. Film hardness, which is defined as the peak indentation force divided by the residual indentation area, was determined for films in the 20nm-thickness range. The residual area was determined from a post indentation scan with scanning force less than 10μN. To determine the final residual area precisely, Lu and Bogy[3] also proposed a method of image registration. The wear resistance of films can also be evaluated in the form of wear depth as a function of the number of scanning wearing cycles[4].

Although these two properties, indentation hardness and abrasive wear resistance, are important in evaluating the mechanical properties of the protective films on disks and sliders, more information is still needed to make a complete evaluation. In addition, since the films of interest are being made thinner, even smaller modifications of the surface (in the 1nm range) are required to avoid loss of resolution due to the substrate effect. However, the PCM method has inherent errors for indentations of this order due to its relatively large tip radius (60-100nm) and the necessity of a post indentation scan. Thus, an improved measurement technique is still needed.

Although hardness is often defined as the peak load divided by the residual indented area, hardness itself is not a fundamental property of material, but rather a

complex combination of properties such as elastic modulus, yield strength, ductility, work-hardening, etc. Hardness is also understood as the resistance to plastic deformation. This resistance involves both elastic and plastic parameters. Thus, the measurement of some additional fundamental properties is important. By using the PCM, hardness values of thin films can be measured, but the elastic modulus and Poisson's ratio can not be, since this method is not able to record the load/displacement curve. With the Hysitron tester, which records the load-unload cycle for each indentation, a reduced composite elastic modulus, which will be defined in Section 3, of the film and substrate can be measured in addition to hardness. With further theoretical analysis, the modulus of the film itself can be separated from the composite value.

After a detailed analysis of hardness and modulii measurement with the Hysitron tester, we use it to study some particular film-substrate systems. The modulus of ultra thin films may not be uniform because they are so thin that grain boundaries, growing directions, dislocations, etc. may play significant roles in the film properties and make them non-homogeneous. A series of tests was made on cathodic arc deposited DLC films to evaluate the dependence of their hardness and modulus on substrate bias and dopant concentration. Tests were also made on a different set of DLC films to study the mechanical properties changes due to annealing. Indentation tests were also made on a homogeneous bulk fused Quartz sample to study the indentation size effect on bulk materials. Results of these tests are presented and discussed.

2. MEASUREMENT ERRORS INHERENT IN THE PCM

Lu *et al*[1], reported an increasing trend of the hardness of polycarbonate and gold with a decrease of indentation force and depth. Figure 1 shows the geometry of a diamond tip used in their indentation hardness measurements by the SPM, where r is the smallest radius of the tip and $2t$ is the lateral dimension of its rounded point. Figure 2 shows a scan of an indentation made by such a tip on a typical surface. Dimensions a and b are the lateral dimensions of the indentation and of the scanned image, respectively. The tip does not follow the surface exactly because of the rounded point. If $a >> t$, the scanned area of order b^2 is roughly equal to the indentation area of order a^2. That means the error introduced by the tip itself is negligible. However, if $a \sim t$, b is much smaller than a. The error introduced by indentation and scanning using such a tip and the associated hardness values are plotted as a function of a in Figure 3, where the indentation mark is assumed to be a circle while a and b represent the diameter of the real mark and that of the scanned mark, respectively. As t/a approaches 1/2, the error tends to infinity because b^2 approaches zero, and therefore the obtained hardness values tend to infinity. When a is larger than about $10t$, that is $t/a < 0.1$, the error is almost negligible. Note that Figure 3 is plotted with a *log-log* scale. This phenomenon can account for the increased hardness measurements in the limit of small indentation depths as observed in Lu *et al*[1].

Since it is very hard to measure the indentation area for such small indentations, methods to obtain relative hardness values by comparing the reciprocal of the residual indentation depths have been proposed. A source of error using this method can be the scanning speed. Figure 4 shows the depths measured by a Hysitron tester, which works

very similarly to the PCM in the scanning mode, with various scanning speeds after an indentation was made. The “Hysitron Measurement” shown in the figure is the residual depth read from the force/displacement curve provided by the Hysitron software. When scanning at larger speeds, the depths obtained are smaller. When scanning at sufficiently low speeds, the depth values are larger and approach the residual depth measurement, but they are not equal to it. In this particular case, scanning at 2 Hz (2 μm/s) takes about 1.5 minutes but scanning at 0.1 Hz (0.1 μm/s) takes about 1 hour to obtain the image. The error in measuring the depth may be caused by the tip’s inability to reach the deepest parts of an indentation mark when scanning at higher speeds. The lower the speed, the more completely the tip sinks to the deepest part. Therefore, obtaining the relative hardness in this way may not be reliable since the real depth is not measured at reasonable scan speeds. An alternative method is needed to measure the hardness values without the errors mentioned above for extremely thin films, i.e. less than 10 nm thick.

3. HYSITRON TESTER AND EXPERIMENTAL METHOD

3.1 Hysitron tester[5]

Figure 5 shows a picture of the Hysitron tester, which was used to perform the indentation tests in this report. The system is a portable add-on to commercially available AFM's. We use it with a Digital Instruments Nanoscope III. It essentially substitutes for the AFM scan head. A schematic diagram of its working mechanism is also shown in Figure 6. The heart of the testing instrument is a three-plate capacitative force/displacement transducer, illustrated in Figure 7. It provides high sensitivity, large dynamic range, and a linear force or displacement output signal. It generates downward forces by changing the capacitance between the plates. The low sprung mass (200mg) of the transducer's center plate minimizes the instrument's sensitivity to external vibrations, and allows very low force indentations to be made. The maximum load that can be applied is approximately 10 mN. The sensor consists of two fixed outer electrodes (drive plates) which are driven by out of phase AC signals. The electric field potential between the plates can be considered to vary linearly, since the drive plates are parallel to each other and closely spaced. Since the signals applied to the drive plates are equal in magnitude but opposite in polarity at any instant, the electric field potential is maximized at the drive plates and minimized at the center plate. Terminals CHA HV IN and CHB HV IN in Figure 7 are used to provide the electrostatic force generated by the transducer. This allows for simultaneous determination of displacement and load during indentation tests. Thus, a load/displacement curve, as shown in Figure 8, can be plotted for an indentation test. Using this result, the information for the material's deformation response to the indentation can be extracted. Material properties like hardness and elastic modulus

can be determined. Figure 9 depicts the Hysitron system in use with a scanning probe microscope. The three blocks on the left side of the diagram (SPM controller, SPM computer and monitor) and the 3-D piezo-actuator are part of the microscope system. The transducer, transducer controller, transducer computer, monitor and signal adapter comprise the Hysitron add-on system.

Various loading functions can be generated through the software supplied with the system. A corner of a cubic diamond tip with a nominal radius of 50 nm is used to indent sample surfaces. Since the tip radius is generally much larger than that of AFM tips, the system can not provide imaging resolutions as high as traditional AFMs. However, the transducers can provide a force output as low as 1 μN. With such a small scanning force, imaging can be easily conducted without deforming the sample surfaces.

3.2 Analysis

Sneddon[6] analytically solved for the elastic stress field within a homogeneous half space when it is indented by a flat rigid punch of a constant contact area. He showed the relationship between the load *P* and the penetration depth *h* for a flat, circular punch is

$$P = \frac{4aGh}{1-\nu} \tag{1}$$

where *a* is the radius of the contact area and G and ν are the shear modulus and Poisson's ratio, respectively. He also showed that a simple relationship exists between the contact stiffness *S*, the projected area of the indentation, or, the contact area *A*, and the elastic modulus *E* that is not dependent on the geometry of the indenter, i.e.,

$$\frac{dP}{dh} = S = 2\sqrt{\frac{A}{\pi}}\left(\frac{E}{1-\nu^2}\right) \tag{2}$$

The term in the parenthesis can be generalized to the reduced modulus E_r , which is defined as

$$\frac{1}{E_r} = \frac{1-\nu^2}{E} + \frac{1-\nu_i^2}{E_i} \tag{3}$$

for non-rigid indenters. S is the stiffness, which is the slope of the unloading curve. Note that for flat punches, the loading and unloading curves should be straight lines, since the contact area stays the same. Oliver and Pharr[7] extended this expression to the deformation behavior of an elastic half space indented by any punch described as a solid of revolution of a smooth function. That means the above expressions can be used even when the contact area between the indenter and the specimen changes continuously as the indenter is withdrawn. They also concluded that this method could be used on the atomic scale. King[8] has studied the validity of Eq. (2) for triangular and square based pyramidal shape indenters by finite element analysis. He concluded that Eq. (2) should be modified to

$$S = \frac{dP}{dh} = 2\sqrt{\frac{A}{\pi}}\beta E_r \tag{2'}$$

where $\beta = 1.034$ for a triangular based pyramid and $\beta = 1.012$ for a square based pyramid. Comparing Eq.(2') and Eq.(2), we see that, $\beta = 1$ for circular cross section indenters. It is apparent that the deviation for the triangular and square geometries from the circular one is only 3.4% and 1.2%, respectively, and thus, Eq.(2) can be used for elastic indentation by indenters which are not true bodies of revolution without generating significant errors.

However, as shown in Figure 8, the indentation tests performed here are not purely elastic processes. The loading process is elastic–plastic, while the unloading process is purely elastic. All of the analysis discussed above is expected to be valid only

for elastic indentations. Further justification is needed to apply it to the current situation. Consider an elastic-plastic load-unload cycle followed by a second indentation on the same spot to the same peak load. As shown in Figure 10, the previously deformed indentation cavity would be deformed again following the previous unloading curve to the same peak load and the same penetration depth. As the load is withdrawn, the material would recover again following the same curve. Thus, the second indentation is purely elastic. However, the initial geometry of the second indentation is quite different from that in Sneddon's flat surface half space solution, as depicted in Figure 11. Tabor[9] found that for a spherical indenter, the elastic load/displacement relation remains the same in a spherical indentation as for the half-space. A subsequent study by Stilwell and Tabor[9] showed the same relation holds for a conical indenter on a conical indentation cavity. Therefore, for these two extreme geometries, (a blunt spherical one and a sharp conical one), Eq.(2) is still valid for elastic indentation cycles. Thus, it is reasonable to extend the use of Eq.(2) to the indenters used in the experiments here, which have spherical heads and conical sides.

As shown in Figure 8, the loading and unloading curves for non-flat indenters are not straight lines, since the contact area changes during the loading and unloading processes. The relation stated in Eq.(2) is valid for any stage of elastic indentation, i.e. it is true on the unloading curve as discussed above. However, during the initial unloading of the indenter, the change of the contact area is very small, which is close to the flat punch model. Eq.(2) is therefore applied to the unloading curve at maximum penetration depth.

Figure 12 shows the geometry of an indentation cross section and parameters for an elastic-plastic indentation. At any stage during the indentation, the total displacement h can be written as $h = h_s + h_c$ where h_s is the elastic displacement of the surface at the perimeter of contact and h_c is the contact depth. The maximum displacement is h_{max}, the surface displacement at the perimeter of contact at maximum depth is h_{sm} and the radius of the contact circle is a at maximum load. After the load is fully withdrawn, the final maximum displacement is h_f. Since a or the contact area A can be related to h_c if the indenter geometry is known, the contact area can be expressed as a function of h_c, i.e.,

$$A = A(h_c) \tag{4}$$

In this way, we can generalize the validity of the analysis to non-circular cross section indenters by finding the function A experimentally. For a perfectly sharp cubic indenter, i.e. with a tip radius of 0,

$$A(h_c) = 2.598 h_c^2 \tag{5}$$

The area functions for indenters in use, which have finite tip radii, will be discussed in the next section. The elastic surface displacement at the perimeter of contact at maximum depth can be determined by following Sneddon's solution for conical indenters,

$$h_{sm} = \frac{\pi - 2}{\pi}\left(h - h_f\right) = \frac{2}{\pi}(\pi - 2)\frac{P_{\max}}{S} = \varepsilon \frac{P_{\max}}{S} \tag{6}$$

where $\varepsilon = 0.72$. For a flat punch, $\varepsilon = 1$, and for a paraboloid of revolution, $\varepsilon = 0.75$. The value of 0.75 will be used for our cubic indenter. Note that this solution already takes care of the possible ridges on the edge of contact. Therefore from the above equation, h_{sm} can be calculated from experimental data at maximum load. Subtracting the surface

displacement h_{sm} from the maximum depth, which is determined from the load/displacement curve, we can find the maximum contact depth. From Eq. (2), the elastic modulus of the material can also be determined. In addition to the modulus, the hardness, which is defined as,

$$H = \frac{P_{\max}}{A}$$

can also be determined. Note that the area A in Eq. (7) is the projected contact area at the peak load. Note also that some authors give the hardness in the same form as in Eq.(7), except that the area used is the final residual indentation area. As indicated by Stilwell and Tabor[10] from their experimental works, after the load is withdrawn, there is an appreciable recovery in depth but there is practically no change in the diameter of the indentation. In other words, the maximum contact area is equal to the final residual indentation area. This means the definition of hardness in Eq.(7) yields almost the same hardness value as that based on the other definition.

3.3 Determination of the initial unloading stiffness

Although it is conceptually easy to find the stiffness from the load/displacement curve, errors can be generated if the data is not interpreted properly. Stiffness is defined as the slope of the tangent line of the unloading curve at the maximum load, and two methods have been proposed to determine the tangent line.

Linear fit:

In the linear fit method, a top portion of the unloading curve is chosen and a linear function, of the form $P = c_1h+c_2$, is fitted to this portion by the least squares method. The slope of this linear function is then said to be the stiffness. Figure 13 shows an example

of a linear fit to the unloading curve. It turns out that the fitted line found in this way is not generally very close to the theoretical tangent line at the maximum load. It can only approximate the theoretical tangent line if a small portion of the unloading curve is chosen. It can be said that this is a first order approximation of the theoretical tangent line. Thus, the linear fit method was not adopted here to calculate the stiffness, except in the cases of very small indentation loads (less than 20μN), in which case signal noise contributes a non-negligible influence on the output data.

Power fit:

Since the linear fit method relies on the proper choice of the top portion of the unloading curve it is necessary to change that portion repeatedly to get a good tangent line at the maximum loading point. A power fit, of the form $P = c\,(h-h_f)^m$, is usually used to fit the top portion of the unloading curve. By differentiating the fitted function analytically, we can calculate the stiffness of the material more accurately. The bottom portion of the unloading curve is usually neglected from the fitting to avoid errors from possible instability while the indenter is just leaving the surface. In this report, 30% of the unloading curve is truncated from the bottom for each calculation.

3.4 Indenter shape function

As noted in the previous section, the area function can be expressed as

$$A = A(h_c) \tag{4}$$

For the indenter shape used in the Hysitron tester Eq. (5) gives the area function for a perfect indenter with a tip radius of zero. However, a real indenter has some finite

tip radius and its area function exhibits some deviation from Eq. (5). An area function with correction terms is suggested as,

$$A(h_c) = 2.598h_c^2 + c_1 h_c + c_2\sqrt{h_c} + c_3\sqrt[4]{h_c} + c_4\sqrt[8]{h_c} + c_5\sqrt[16]{h_c} \tag{5}$$

The leading term describes a perfect indenter; the others represent the deviation from a perfect geometry. To find the coefficients c_1 through c_5 we must make a series of tests. For this purpose bulk fused Quartz was used as a standard sample for its homogenous and isotropic material behavior. The elastic modulus and Poisson's ratio for quartz are 70 GPa and 0.3, respectively. A series of indentations was made within a certain range of contact depths. Shape constants c_1 through c_5 were determined by fitting Eq.(5) to the measured data. Since the curve-fitting technique was applied the values of the area are only valid in the test range. Therefore, the range was chosen to be the working range for future usage. However, if the working range is too large, a significant error is possibly induced by the approximated area function. In this case, two sets of coefficients should be chosen for the application to larger and smaller contact depths. Under the assumption that the elastic modulus is constant and independent of the contact depth, the area can be calculated for each indentation by substituting the material properties and the stiffness into Eq. (2). Figure 14 shows the area vs. contact depth for tip 20, which has a nominal tip radius of about 50 nm. The fitted curve is also shown in the figure. The solver in Microsoft Excel was used to determine the best fitting coefficients. The five coefficients for tip 20 were found to be: -1.497, 2.584, -3.861, 3.718, -1.482. For this particular calibration, the working range is from 5 nm to 75 nm. Generally speaking, these coefficients would not change if the indentations are made on materials with hardnesses under 40GPa. They do change very slightly if a series of indentations is made

on materials harder than 40GPa, due to the deformation of the diamond tip. So these coefficients should be checked periodically, for example, every 100 indentations if the tip is used for hard material indentations.

It is also possible to obtain the shape functions for various nominal tip radii with the same tip shape. Thus, the radius of a tip can be roughly interpolated by using previously determined shape functions.

3.5 Correction for thin film indentation

The method described above works well for indentation on bulk samples. But only the composite material properties are determined in this manner if indentation is performed on multi-layered materials when indentation depths exceed 10 to 20 percent of the layer thickness. To solve this problem, Doerner and Nix[11] introduced an effective contact modulus, $[(1-\nu)/G]_{eff}$, expressed as some linear combination of the modulus of the film and that of the substrate. King[8] adopted an integral equation analysis and modified Doerner and Nix's equation to fit his experimental results. Ramsey[12] employed a plate on an elastic foundation subjected to a point force model. He discussed the cases for both small deflection and large deflection. Parallel to the above studies, finite element methods have also been used to simulate indentation tests (Bhattacharya and Nix[13], Laursen and Simo[14]). Lu and Bogy[15] studied the effect of tip radius on hardness values of soft/hard (Al/Si) and hard/soft (Si/Al) thin film systems.

Gao *et al*[16], applied a first order modulii-perturbation method to the multi-layer material problem. They assumed the film/substrate medium could be viewed as a homogeneous body made entirely of the substrate material subjected to a phase transformation in the film region. During the transformation the applied force P is kept

constant, but the vertical displacement h and strain energy are allowed to change. Energy conservation requires that the extra work done by the force P be equal to the energy change in the whole body. Then the effective shear modulus and Poisson's ratio can be expressed as

$$G_{eff} = G_s + (G_f - G_s) I_0(\xi)$$

$$\nu_{eff} = \nu_s + (\nu_f - \nu_s) I_1(\xi) \tag{10}$$

Where $\xi = t/a$, t is the film thickness and a is the radius of the contact circle for a conical indenter. Moreover, the functions I_0 and I_1 are given by

$$I_0(\xi) = \frac{2}{\pi}\tan^{-1}\xi + \frac{1}{2\pi(1-\nu)}\left[(1-2\nu)\xi \ln\left(\frac{1+\xi^2}{\xi^2}\right) - \frac{\xi}{1+\xi^2}\right] \tag{11}$$

$$I_1(\xi) = \frac{2}{\pi}\tan^{-1}\xi + \frac{\xi}{\pi}\ln\left(\frac{1+\xi^2}{\xi^2}\right) \tag{12}$$

Both I_0 and I_1 approach 0 as ξ approaches 0 and they approach 1 as ξ approaches infinity, as indicated in Figure 15. I_0 can also be interpreted as the ratio of strain energy stored in the transformed region to the total strain energy stored in the half space. Thus, G_{eff} can be viewed as an average shear modulus weighted by the strain energy density distribution. I_1 is also regarded as the ratio of the dilatational strain energy stored in the transformed (film) region to the total dilatational strain energy. In addition, ν_{eff} is an average Poisson's ratio weighted by the dilatational strain energy distribution. From Eq. (9) and Eq. (10), the effective elastic modulus can be determined by assuming the Poisson's ratio of the film is close to that of the substrate.

$$E_{eff} = 2\left[\frac{E_f}{2(1+\nu_f)} I_0 + \frac{E_s}{2(1+\nu_s)}(1-I_0)\right] \cdot \left[1 + \nu_f I_1 + \nu_s (1-I_1)\right]$$

$$= E_s + (E_f - E_s) I_0 \tag{14}$$

Notice that I_0 is a function of the film thickness, which has to be known before any calculation can be made. The total vertical displacement of the film/substrate system under indentation is also given as

$$h(\xi) = \frac{P(1-\nu_s)}{4aG_s}\left[1 - \frac{\nu_f - \nu_s}{1-\nu_s} I_1(\xi) - \frac{G_f - G_s}{G_s} I_0(\xi)\right] \tag{15}$$

Gao *et al*[16] also showed that Eq. (15) can be generalized to a multi-layered system by rewriting it as

$$h(\xi) = \frac{P}{4a} \cdot \frac{1 - [1 - I_1(\xi_n)]\,\nu_s - \sum_{i=1}^{n} [I_1(\xi_i) - I_1(\xi_{i-1})]\,\nu_i}{[1 - I_0(\xi_n)]\,G_s + \sum [I_0(\xi_i) - I_0(\xi_{i-1})]\,G_i} \tag{16}$$

The general solution for a rigid punch indenting a nonhomogeneous material with continuously varying modulii can also be obtained by taking the limits $n \to \infty$ and $\xi_i \to \xi_{i-1}$

$$h(\xi) = \frac{P}{4a} \frac{1 - \int_0^\infty \frac{dI_1(z/a)}{dz} \nu(z) dz}{\int_0^\infty \frac{dI_0(z/a)}{dz} G(z) dz} \tag{17}$$

Gao *et al*[16] showed that Eq. (11) and Eq. (12) match with the elastic FEM simulation results very well. Thus, Eq. (11) through (15) are adopted in the analysis in section 4. Note that a is the radius of the contact circle for conical indenters. For the cubic indenter used in the Hysitron tester, a needs to be replaced by $(A/\pi)^{1/2}$ in which A is the contact area between the indenter and the material.

4. EXPERIMENTAL RESULTS AND DISCUSSIONS

4.1 Indentation tests on bulk fused Quartz

A series of indentation tests were performed on bulk fused Quartz to verify that there is no indentation depth effect when using the Hysitron tester with the method of analysis discussed in section 2. Figure 16 shows the hardness values of fused Quartz vs. various contact depths. Here we do not see a trend of increased hardness when the contact depth gets smaller. The average hardness value is about 10 GPa, which is very close to the reported hardness for Quartz.

4.2 Nano-hardness tests on WC_x films: bias and W concentration effects

The need for thinner overcoat films with better wear and corrosion protection properties for hard magnetic disk applications supports much research in film deposition processes and optimization. Amorphous carbon films (often referred to as diamondlike carbon or DLC) have been most widely used. It was recognized early that even the best DLC has limited application at temperatures above 300°C, because of the degeneration of its properties. On the other hand, it has been reported that the flash temperature at the contact point between a slider and the disk can be as high as 1000°C in the contact-start-stop mode of operation of a hard drive. In order to produce hard films that can sustain their properties at such elevated temperatures, some researchers have incorporated dopants in DLC films. The reason for this approach is that, in general, carbides are chemically stable and maintain good mechanical properties at elevated temperatures. In particular, WC is known to have a high hot hardness.

The WC_x films used in this study were deposited by the Dual-Source Metal Plasma Immersion Ion Implantation and Deposition Method by Dr. Othon Monteiro at the Lawrence Berkeley National Laboratory[17]. In this method the films are produced by mixing streams of W^+ and C^+ ions produced by two repetitively pulsed vacuum arc plasma sources operating synchronously, and negatively pulse-biasing the substrate, which is Silicon <100>. In order to achieve a smooth surface, free of microparticles, the plasma streams are magnetically filtered, and the substrate is placed out of the line-of-sight of the cathode. In the deposition apparatus, a master pulse generator was used to gate the arc supplied by the individual plasma sources, as well as the high voltage power supply for the substrate biasing. Each arc supply can sustain the arc for a predetermined duration. Both arcs were triggered simultaneously, and last for a specific length of time. The repetition rate of the pulses was 1 Hz. The composition of the films was controlled by varying the duration of the arc in each source during the pulses according to the values shown in Table I. This table also shows the applied bias voltage and the final film thickness. The film composition was investigated by Auger electron spectroscopy (AES), X-ray photoelectron spectroscopy (XPS) and Rutherford backscattering spectroscopy by Monteiro *et al*[17], and is summarized in Table II.

A series of indentation tests was performed on these WC_x films using the Hysitron tester. In order to avoid substrate effects, we performed the indentations such that the residual indentation depths were kept below 20% of the film thickness, which is about 4 to 5 nm, since the films thicknesses are around 20 nm. The hardness of the film that was grown under –100V bias and zero W concentration was also measured for comparison, and it was found to be 73 GPa. The measured hardness values of the samples

deposited with a bias of –100V are shown in Figure 17. Each point in the figure represents the average of three measurements. As shown, the addition of a small amount of W to an undoped DLC results in a significant reduction in hardness. An addition of 0.8 atomic percent of W reduces the hardness from 72 GPa to 63 GPa. The introduction of more W causes a further reduction in hardness. With a 10% W concentration, the hardness can be as low as 35 GPa. Similar observations can be made from Figure 18 and Figure 19 for films deposited with a bias of –500V and –2000V, respectively. Again, each point in these two figures represents the average of three measurements. Comparing Figure 17 to Figure 19, we see that films with higher negative bias generally have smaller hardness values. The hardness of the film with the highest bias (-2000V) and largest W concentration (10%) can be as low as 20 GPa, which is less than a third of the hardness of the film without bias and W concentration.

Monteiro[17] has measured the internal stresses in these films. He showed a trend of decreasing internal stress with an increase of W concentration and substrate bias. He also concluded that the inclusion of W reduces the formation of sp^3 bonding and produces sp^2 bonding. In addition, a large substrate bias favors the growth of the sp^2 bonding, which reduces the internal stress in the films.

The correlation of the internal stress and hardness can be understood by the Mohr's circle technique, as depicted in Figure 20. The radius of the circle is considered to be some fixed value, which could be similar to the yielding stress. Note that the hardness can be understood as the average stress that causes plastic deformation, which is the magnitude of the compressive stress the indenter generates. A larger compressive residual stress associated when film deposition would result in a higher hardness value, since it

would move the Mohr's circle towards the left-hand side. A tensile stress would move the circle towards the right and thus, result in a lower hardness value.

4.2 Modulii of DLC films: thermal stability

DLC films deposited by the Vacuum Cathodic Arc method were heated to 900°C in the same vacuum chamber to determine the change in their material properties after annealing. Figure 21 shows the hardness measurements for samples A and B, which were both deposited with –100V substrate bias. Their thickesses are about 30nm. After deposition, Sample B was heated to 900°C in the same chamber and cooled down to room temperature, while sample A remained at room temperature without annealing. Sample B exhibits a substantial increase in hardness at the contact depth of about 10 –12 nm. It goes up to 110 GPa at the contact depth of 10.2 nm. The hardnesses for both samples decrease with similar values as the contact depth increases, since the effect from the substrate become more dominant. Since the hardness of the diamond indenter used in this test is about 90 GPa, which is very close to the DLC film hardness, further analysis may be needed to compensate for the deformation of the indenter.

Figure 22 shows the elastic modulii of the two samples. The lower two curves represent the composite film modulii with the substrate effect. The upper ones indicate the pure film modulii determined by the decomposition method discussed in section 3. It is not surprising that the film modulii are not invariant to changes in the contact depth, since the material properties are not generally uniform for thin films.

Raman Spectroscopy and Near Edge X-Ray Absorption Fine Structure (NEXAFS) spectroscopy were performed on these two samples by Anders *et al*[18]. The

Raman aperture was observed to be practically unchanged after annealing, although there may be a very small shoulder around 1350 cm^{-1} indicating the beginning of the graphic D-band. The NEXAFS results showed a slight modification (graphitization) of sample B. This discrepancy could be explained by the surface sensitivity of NEXAFS whereas Raman spectroscopy and nanoindentation integrate over the whole film thickness.

Figure 23 shows the indentation force/displacement curves for sample B. It is worth noting that there is a slope change in all loading curves at the 30 nm contact depth. This is possibly an indication of material yielding, cracking, or just full penetration of the film. To clarify this point, a tip with a different tip radius is needed to generate different stress levels under the tip. If the slope change point moves, then this point is likely to be due to yielding or cracking. If not, then this point may represent full penetration of the film and the remaining part of the loading curves represent the force/displacement relation for the substrate.

5. SUMMARY AND CONCLUSIONS

The Hysitron tester is capable of performing nanoindentation tests on bulk materials. It can also be used to characterize thin films with thicknesses less than 20nm, since it can generate indentation forces as low as 10μN with noise of smaller order. When employed with a proper theoretical analysis, the system does not require a post-indentation imaging to get the indentation area and the indentation depth. Therefore, no instrument error is generated while assessing the hardness of materials. Since it records force and displacement data during loading and unloading of the indentation, it can also be used to evaluate the modulus of bulk materials and the composite elastic modulus of the film and substrate. However, a new diamond indenter cannot be used in its virgin state. Before using it, a tip shape calibration procedure must be performed. If tests are mainly done on relatively soft materials (30~40 GPa), shape constants can last for a large number of indentations. If tests are mainly done on relatively hard materials (>40 GPa), shape constants need to be checked periodically, since the shape of the indenter changes due to its fairly large plastic deformation while indenting on hard materials. This is not a concern if interest is mainly on disk and slider overcoats, since the hardnesses in question are around 20 to 30 GPa. Note that an indenter used for indentation tests should not be used to wear or scratch film surfaces without re-calibration, since wearing and scratching would change its shape.

The hardness values of W doped DLC films decrease with the increase of W concentration and the increase of the magnitude of the negative bias. With a 10% W concentration in the film, the hardness drops to 35 GPa, about half of the hardness of the W-free film. At low W concentration, the increase in the negative substrate bias drops the

film hardness significantly. However, at high W concentration, the effect of substrate bias on film hardness is weaker.

There was no observed effect of annealing to 900°C on the hardness and modulus of DLC films. The annealed film has a maximum hardness below the surface. The hardnesses of both films decrease as the contact depth increases due to the substrate effect. With the help of the analysis method discussed in section 3, the film modulii can also be determined from the composite modulii. For the films tested, the elastic modulii changed with changes in the contact depths.

No indentation size effect was found on the bulk fused Quartz sample using the Hysitron tester.

Table I: Deposition parameters and thickness of the WC_x films produced by Dual-Source MePIIID. (Arc currents during the pulses were: I_c = 270 A, I_w = 170A)

Sample	Arc Duration (ms) C gun	Arc Duration (ms) W Gun	Substrate bias Voltage (V)	Film Thickness (nm)
517	5.0	2.5	-100	26
518	5.0	2.5	-500	30
519	5.0	2.5	-2000	18
520	5.0	1.0	-100	27
521	5.0	1.0	-500	30
522	5.0	1.0	-2000	46
523	5.0	0.5	-100	44
524	5.0	0.5	-500	40
525	5.0	0.5	-2000	50

Table II: Composition of the WC_x films

Arc Duration (ms) C	Arc Duration (ms) W	C fraction	W fraction
5.0	2.5	0.9	0.1
5.0	1.0	0.96	0.04
5.0	0.5	0.992	0.008

REFERENCES

[1] C. J. Lu, D. B. Bogy, and R. Kaneko, “ Nanoindentation hardness tests using point contact microscope”, *J. Tribol*. Vol. **116,** 175-80(1994)

[2] R. Kaneko, K. Nonaka, and K. Yasuda, “Scanning tunneling microscope and atomic force microscopy for microtribology”, *J. Vac. Sci. Technol.* Vol. **A6**, 291-2(1988)

[3] C. J. Lu and D. B. Bogy, “Sub-microindentation hardness tests on thin film magnetic disks”, *Advances in Information Storage Systems* Vol. **6**, 163-75(1995)

[4] Z. Jiang, C. J. Lu, D. B. Bogy, C. S. Bhatia, and T. Miyamoto, “Nanotribological characterization of hydrogenated carbon films by scanning probe microscopy”, *Thin Solid Films*, Vol. **258**, 75-81(1995)

[5] Hysitron Triboscope Users Manual

[6] I. N. Sneddon, “The relation between load and penetration in the axisymmetric Boussinesq problem for a punch of arbitrary profile”, *Int. J. Eng. Sci*., No. **3**, 47-57(1965)

[7] G. M. Pharr, W. C. Oliver and F. R. Brotzen, “On the generality of the relationship among contact stiffness, contact area, and elastic modulus during indentation” *J. Mat. Res*. Vol. **7**, No. **3**, 613-17(1992)

[8] King, R. B., “Elastic analysis of some punch problems for a layered medium”, *Int. J. Solids and Structures*, Vol. **23**, No. 12, 1657-64(1987)

[9] D. Tabor, “A simple theory if static and dynamic hardness”, *Proc. Roy. Soc.* **Vol. A 192**, 247-74(1948)

[10] N. A. Stilwell and D. Tabor, “Elastic recovery of conical indentations”, *Proc. Phys. Soc. Lond.* **Vol. 78**, 169-79(1961)

[11] M. F. Doerner, and W. D. Nix, “A method for interpretating data from depth-sensing indentation instruments”, *J. Mat. Res*. Vol. **1**, 601-9(1986)

[12] P. M. Ramsey, “Modeling the contact response of coated systems*”, Surface and Coatings technology*, Vol. **49**, 504-9(1991)

[13] Bhattacharya, A. K. and Nix, W. D., “Analysis of elastic and plastic deformation associated with indentation testing of thin films on substrates”, *Int. J. Solids and Structures*, Vol. **24**, No. **12**. 1287-98(1988)

[14] Laursen, T. A. and Simo, J. C., “A study of the mechanics of microindentation using finite elements”, ”, *J. Mat. Res*. Vol. **7**, 618-26(1992)

[15] C. J. Lu and D. B. Bogy, “The effect of tip radius on nano-indentation hardness tests”, *Int. J. Solids and Structures*, Vol. **32**, No. 12, 1759-70(1995)

[16] Huajian Gao, Cheng-Hsin Chiu, and Jin Lee, “Elastic contact versus indentation modeling of multi-layered materials”, *Int. J. Solids Structures* Vol. **29**, No. 20, 2471-92(1992)

[17] O. R. Monteiro, “Synthesis and characterization of thin films of WCx produced by mixing W and C plasma streams”, accepted by *Surface and Coatings Technology*, (1997)

[18] S. Anders, Javier Diaz, and Joel W. Ager III, “Thermal stability of amorphous hard carbon films produced by cathodic–arc deposition”, submitted *to Applied Physics Letters,* (1997)

[19] Shefford P. Baker, “The analysis of depth-sensing indentation data”, *Mat. Res. Soc. Sym. Pro.*, Vol. **308**, 209-19(1993)

[20] T. J. Lardner, J. E. Ritter, H. B. Karamustafa, “Effect of the substrate on microindentation behavior”, *Mat. Res. Soc. Sym. Pro*., Vol **308** 189-94(1993)

[21] N. J. Mccormick, M. G. Gee, D. J. Hall, “The calibration of the nanoindenter”, *Mat. Res. Soc. Sym. Pro.*, Vol **308** 195-200(1993)

[22] C. J. McHargue, “Surface mechanical properties using nanoindentation”, *Micro/Nanotribology and its applications*, edited by B. Bhushan, 467-92(1997)

[23] M. E. O’Hern, W. C. Oliver, C. J. McHargue, D. S. Rickerby, S. J. Bull, “The hardness and elastic modulus of thin films as determined by ultra-low load indentation”, *Mat. Res. Soc. Sym. Pro.*, Vol. **188**, 139-43(1993)

[24] J. S. Field and M. V. Swain, “A simple predictive model for spherical indentation”, *J. Mat. Res*. Vol. **8**, 297-306(1993)

[25] W. C. Oliver, G. M. Pharr, “An improved technique for determining hardness and elastic modulus using load and displacement sensing indentation experiments”, *J. Mat. Res.*, Vol **7**, No. **6**. 1564-83(1992)

[26] W. H. Poisl, B. D. Fabes, W. C. Oliver, “A quantitative model for interpreting nanometer scale hardness measurements of thin films”, *Mat. Res. Soc. Sym. Pro*., Vol **308,** 201-208(1993)

[27] C. W. Shih, “Effect of tip radius on indentation”, *J. Mat. Res*., Vol **6**, No. **12**, 2623-28(1991)

[28] Haifeng Wang and Herwig Bangert, “Study of bulk and film-substrate composite material behavior under Vickers indentation by three-dimensional finite element simulation”, *Mat. Res. Soc. Sym. Pro*., Vol **308,** 183-8(1993)

[29] T. P. Weihs, “Mechanical deflection of cantilever microbeams: A new technique for testing the mechanical properties of thin films”, *J. Mat. Res*. Vol. **3**, No. 5, 931-42(1988)

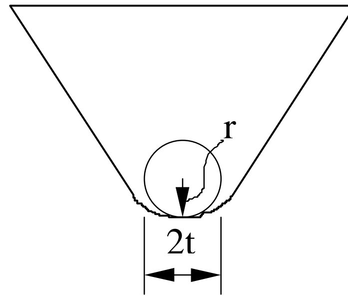

Figure 1: The geometry of a diamond tip

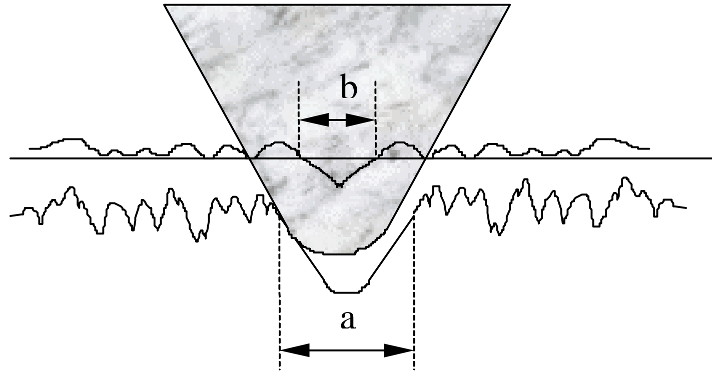

Figure 2: The schematic trajectory of a tip on a rough surface

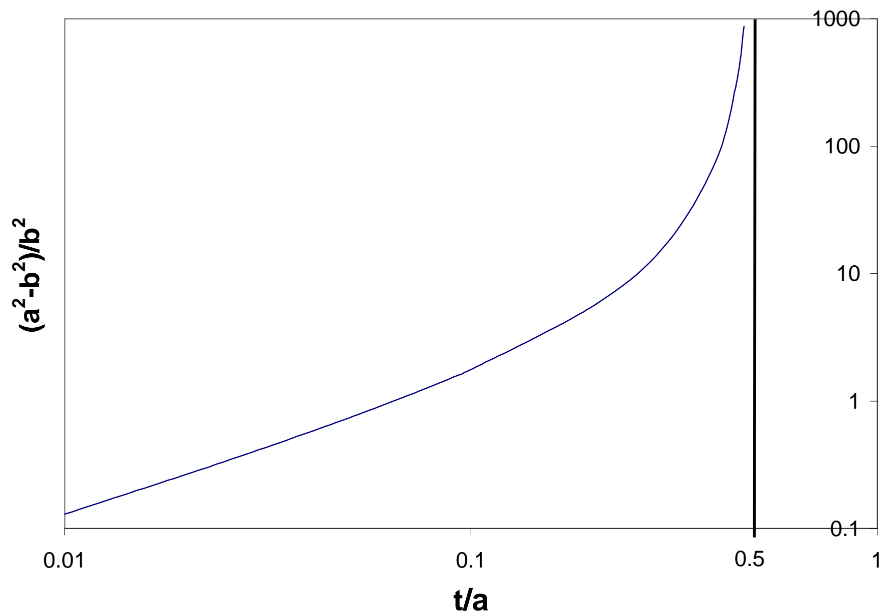

Figure 3: Error introduced by finite tip radius

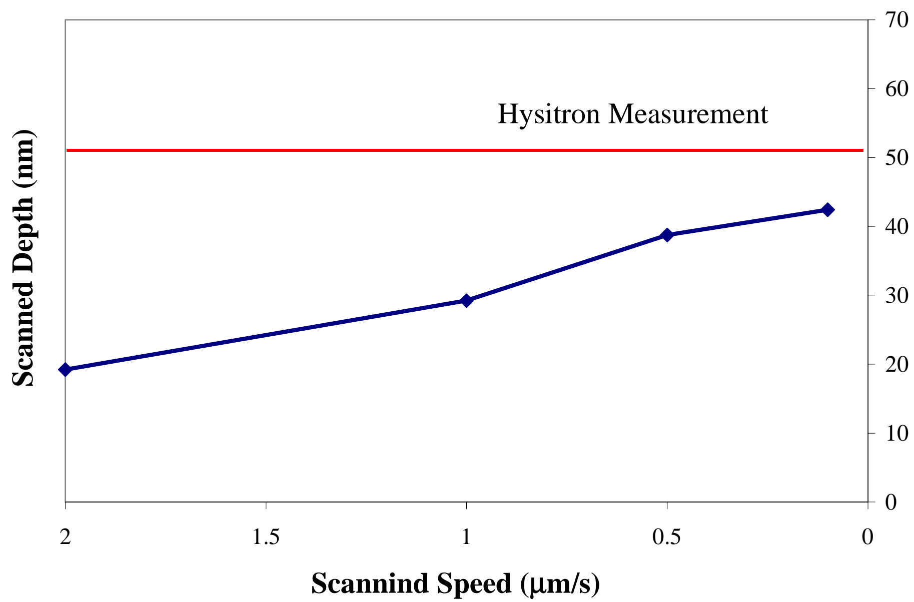

Figure 4: Scanned depth by Hysitron Picotester of the same indentation mark. The "Hysitron Measurement" is read from the force/displacement curve.

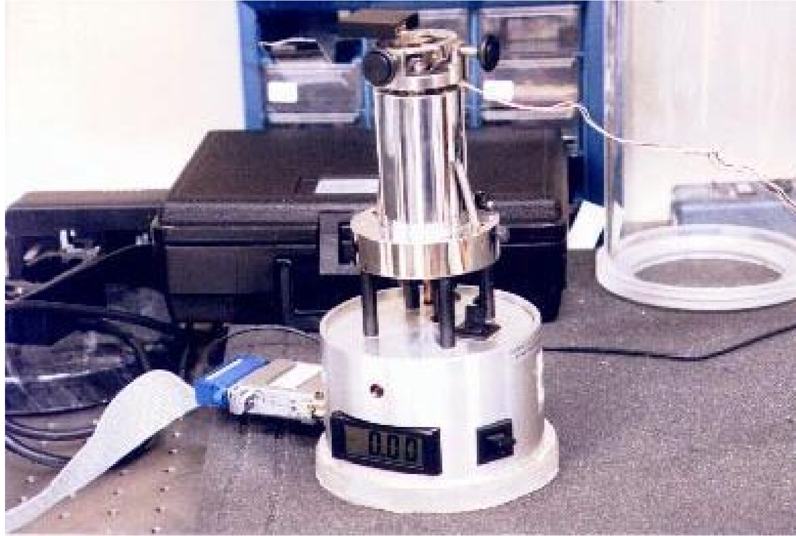

Figure 5: A picture of the Hysitron tester sitting on the top of an AFM

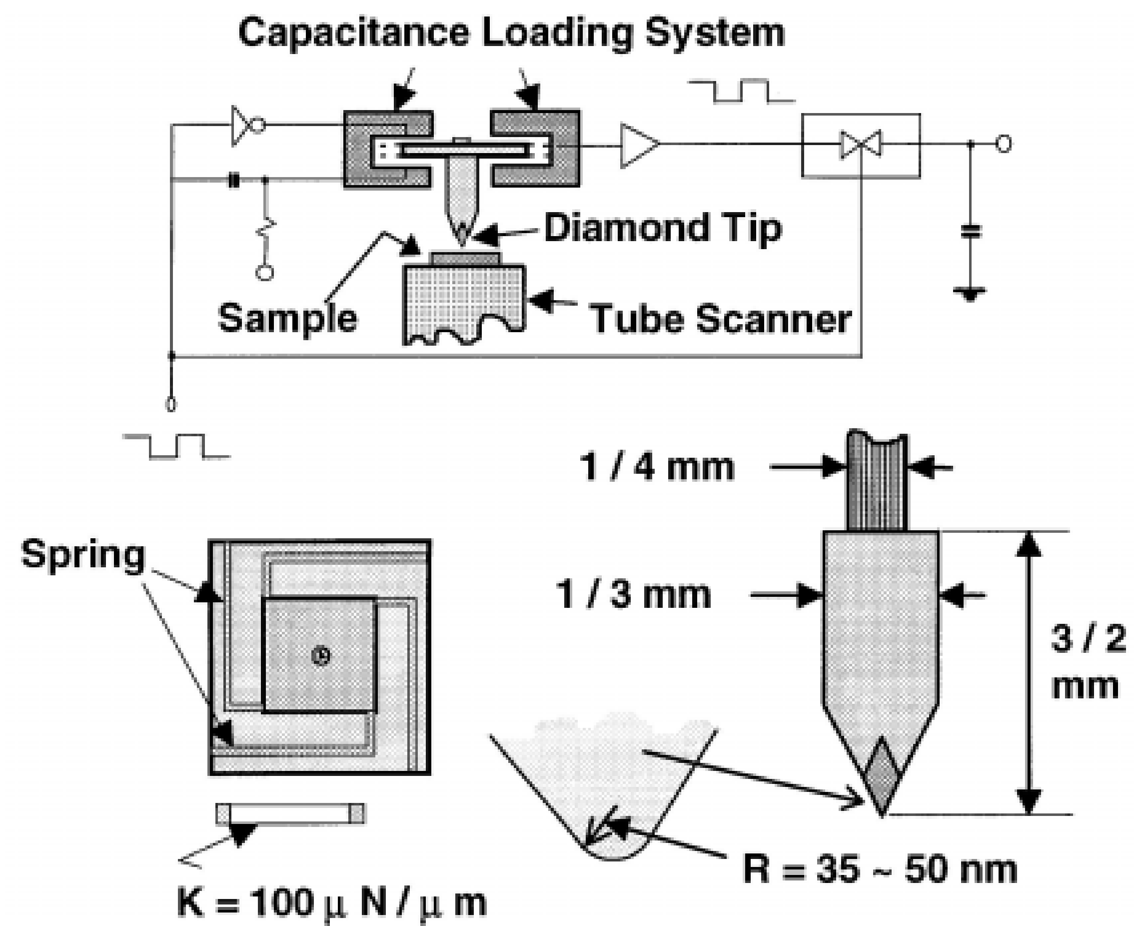

Figure 6: The schematic diagram of the working mechanism of the Hysitron tester

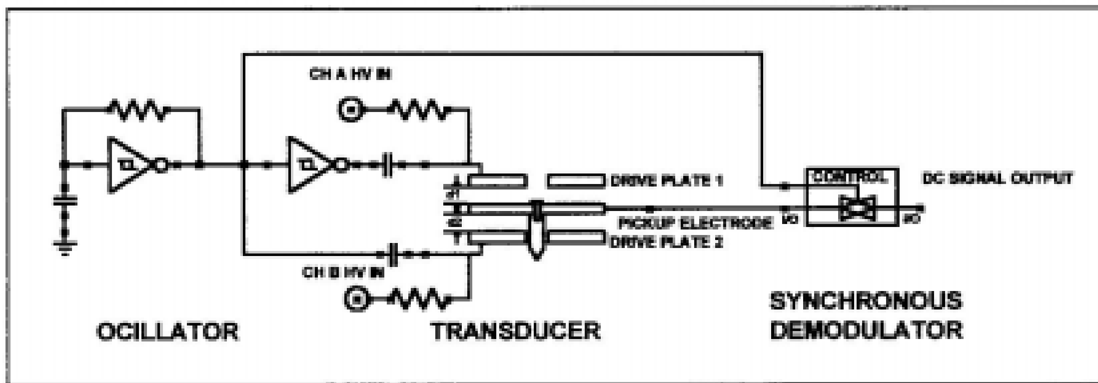

Figure 7: Three-plate capacitative design

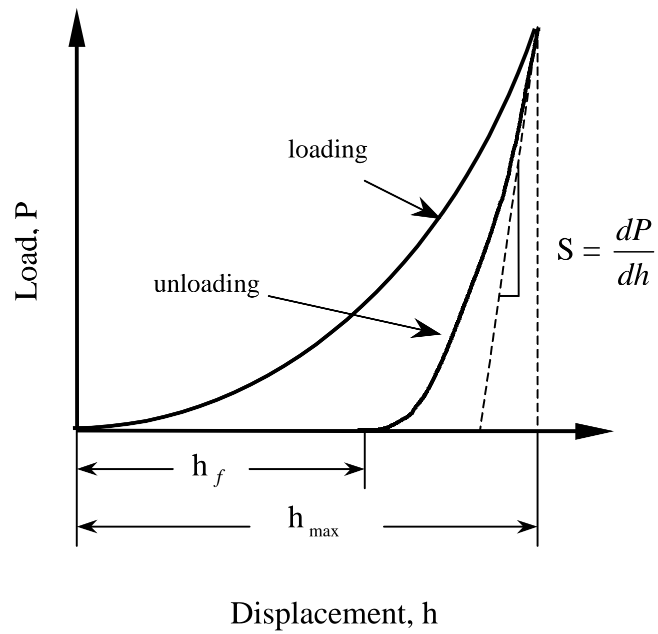

Figure 8: Typical load/displacement curve for an indentation

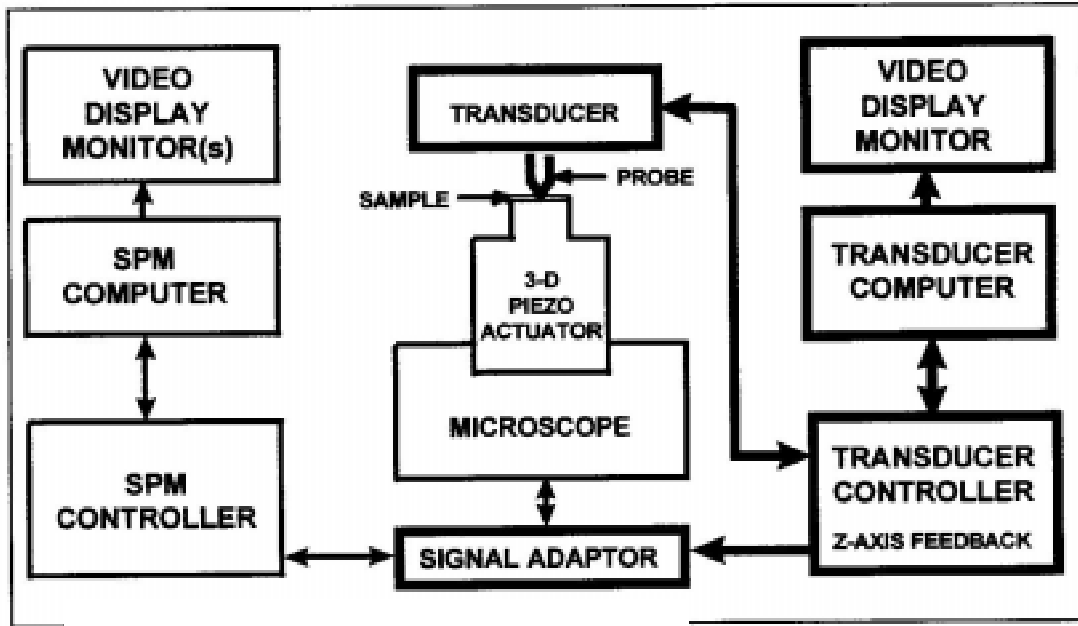

Figure 9: Block diagram of the Hysitron system

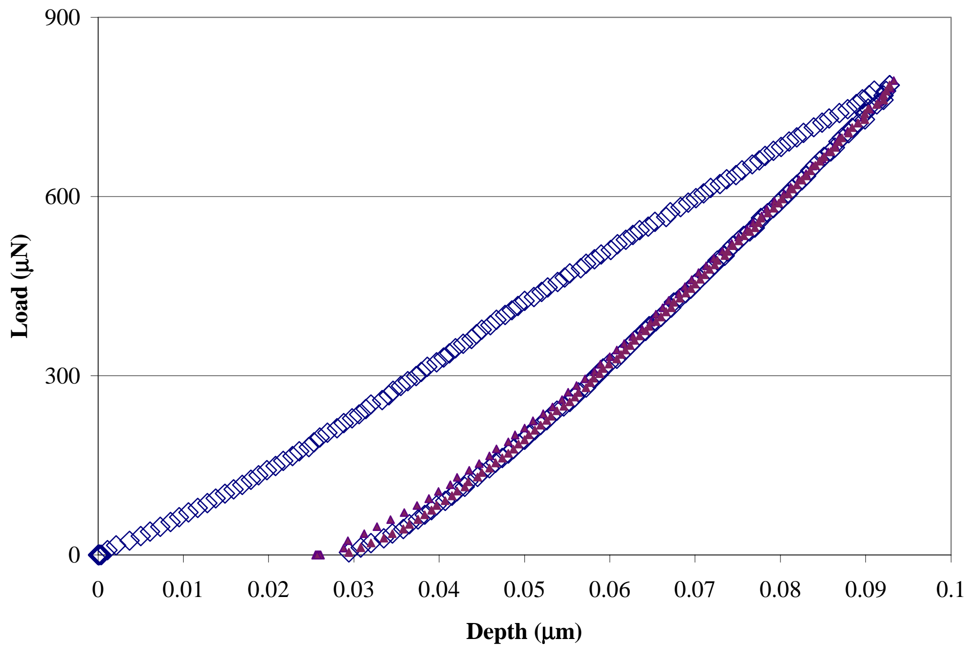

Figure 10: Second indentation on a previously indented spot.

Flat surface half space

Indented cavity surface

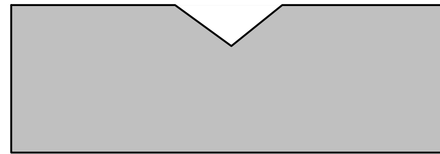

Figure 11: Flat surface half space in Sneddon's solution and the indented surface.

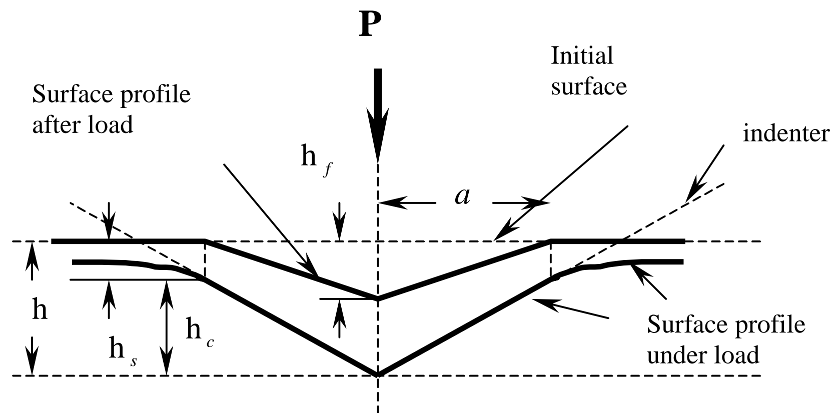

Figure 12: The geometry of an indentation cross section and parameters of an elastic-plastic indentation

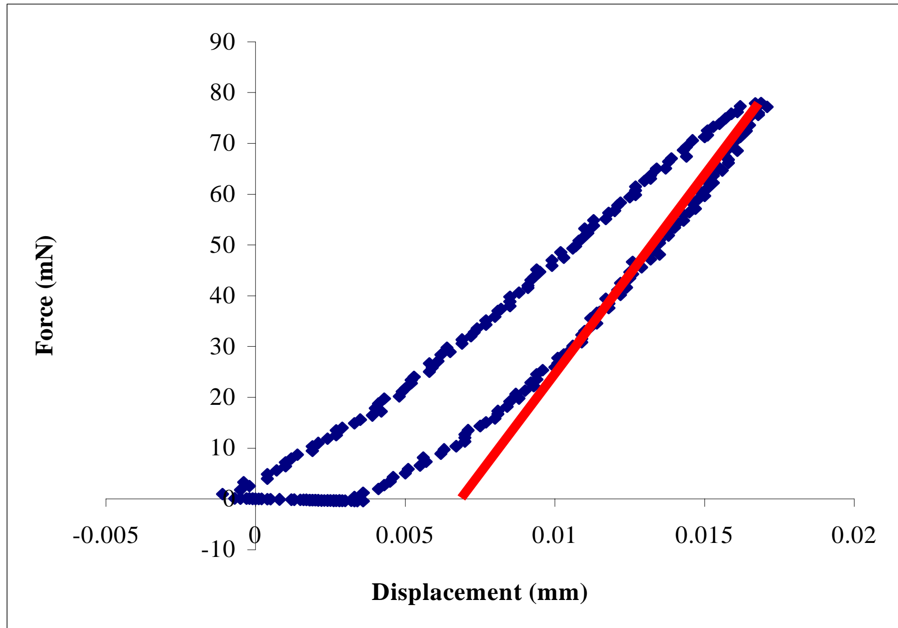

Figure 13: A linear fitting line to the unloading curve

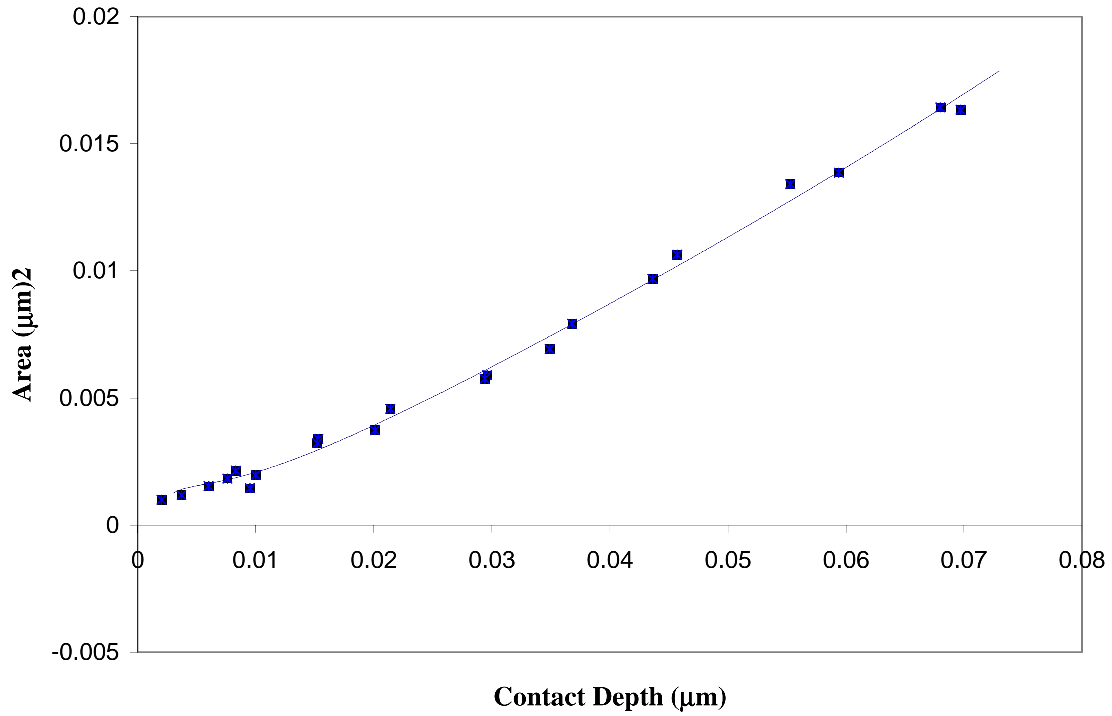

Figure 14: the Calibration Curve for Tip 20

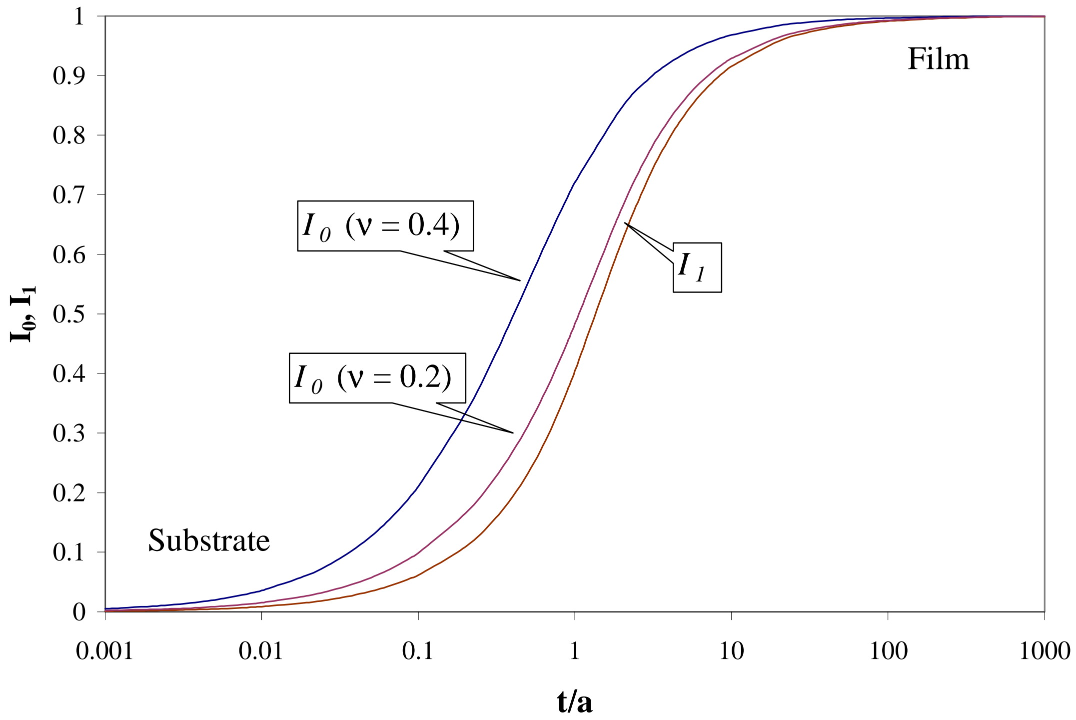

Figure 15: I_0 and I_1 function

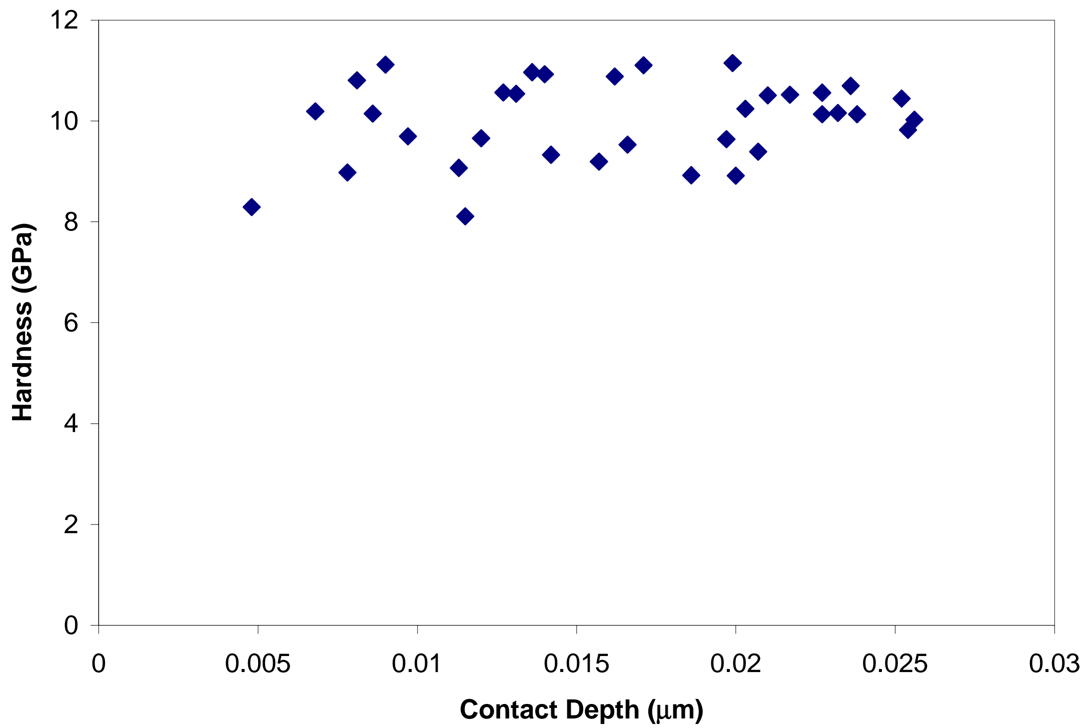

Figure 16: Hardness of bulk fused Quartz

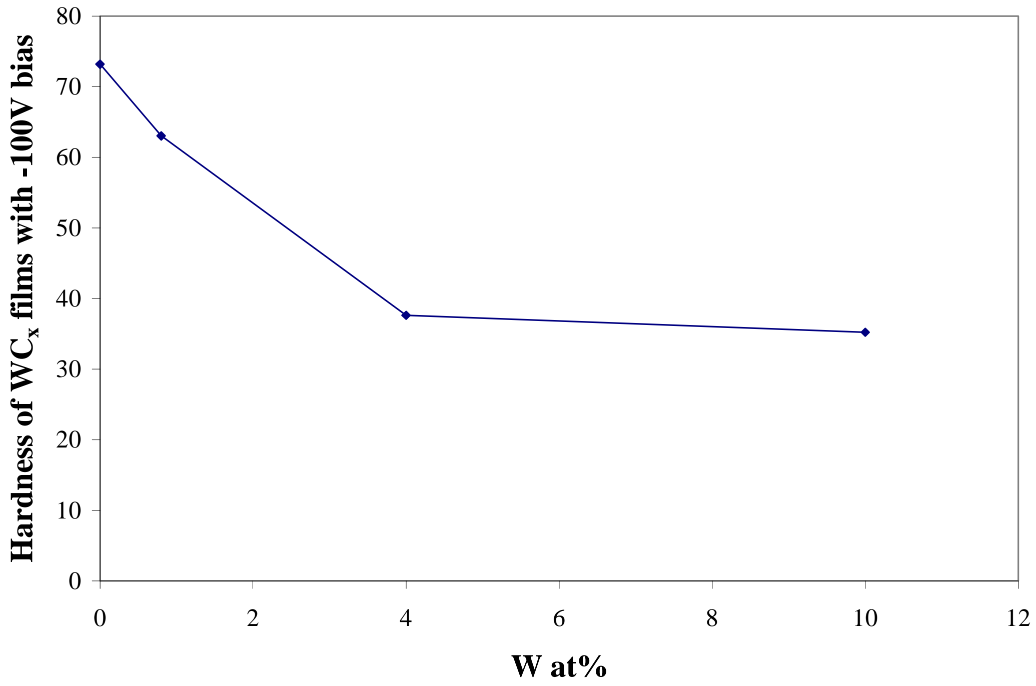

Figure 17: Hardness of WC_x films with –100V substrate bias

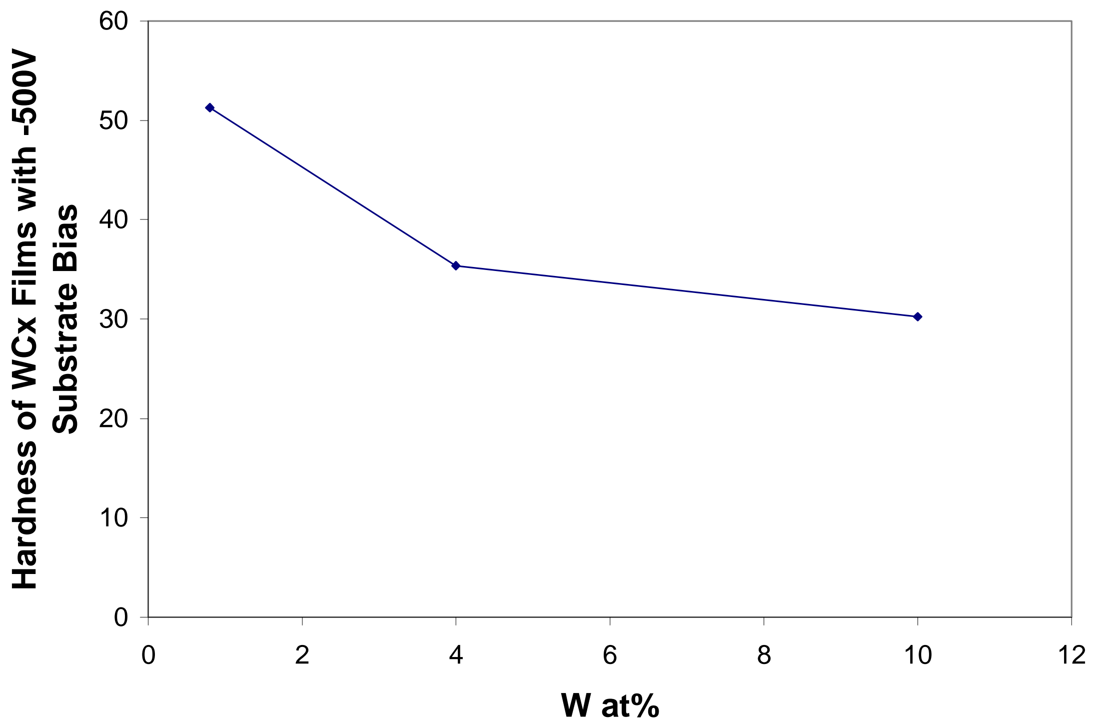

Figure 18: Hardness of WC_x films with –500V substrate bias

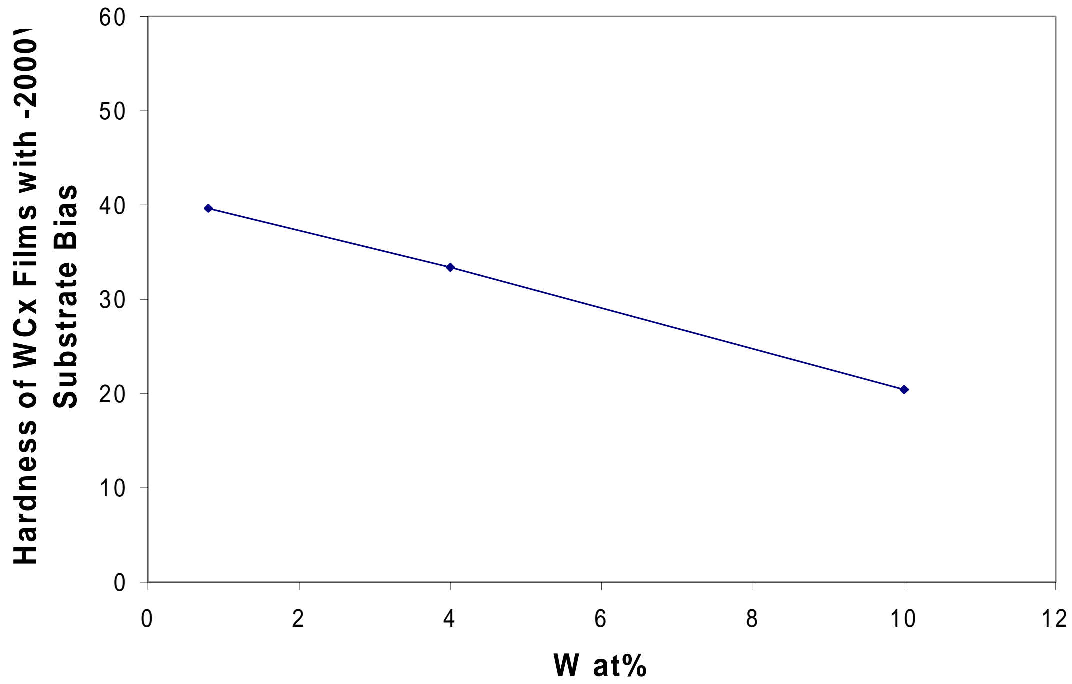

Figure 19: Hardness of WC_x films with –2000V substrate bias

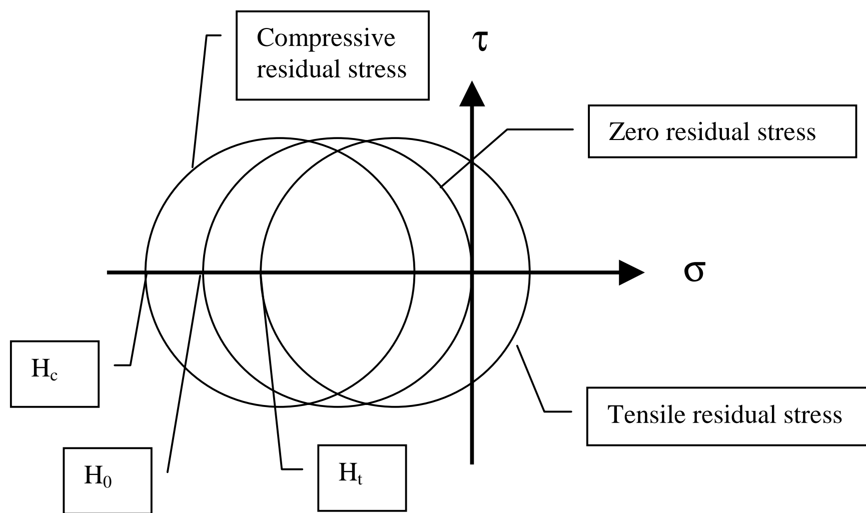

Figure 20: Mohr's circle interpretation of the effect of residual stress on the hardness, where τ is the shear stress and σ is the normal stress

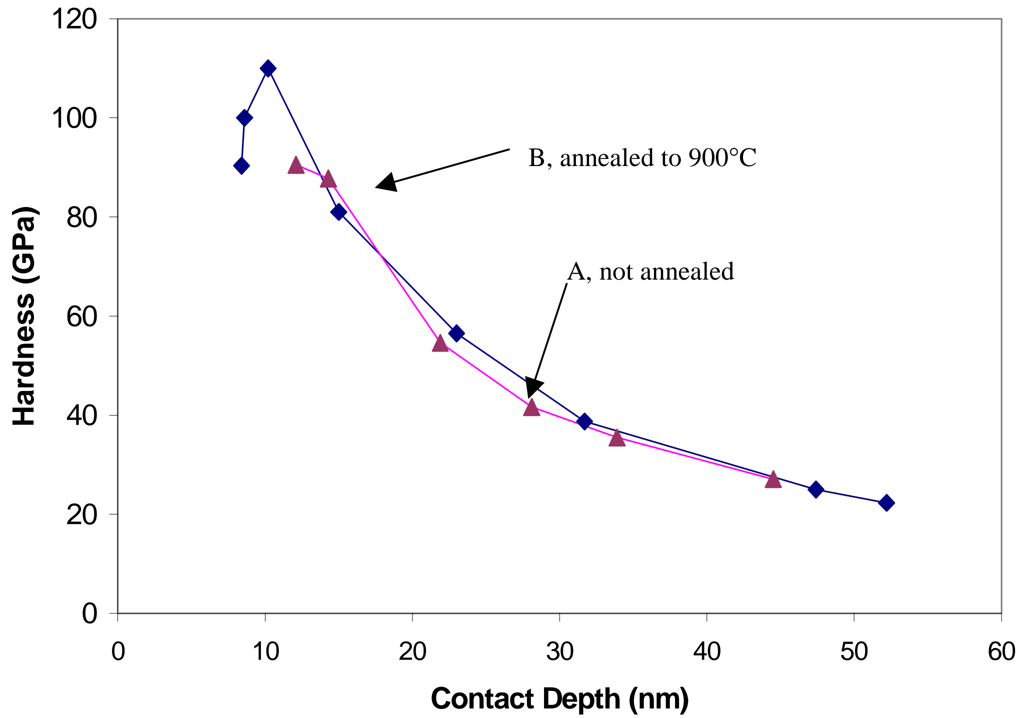

Figure 21: Hardness of Annealed and un-annealed DLC samples

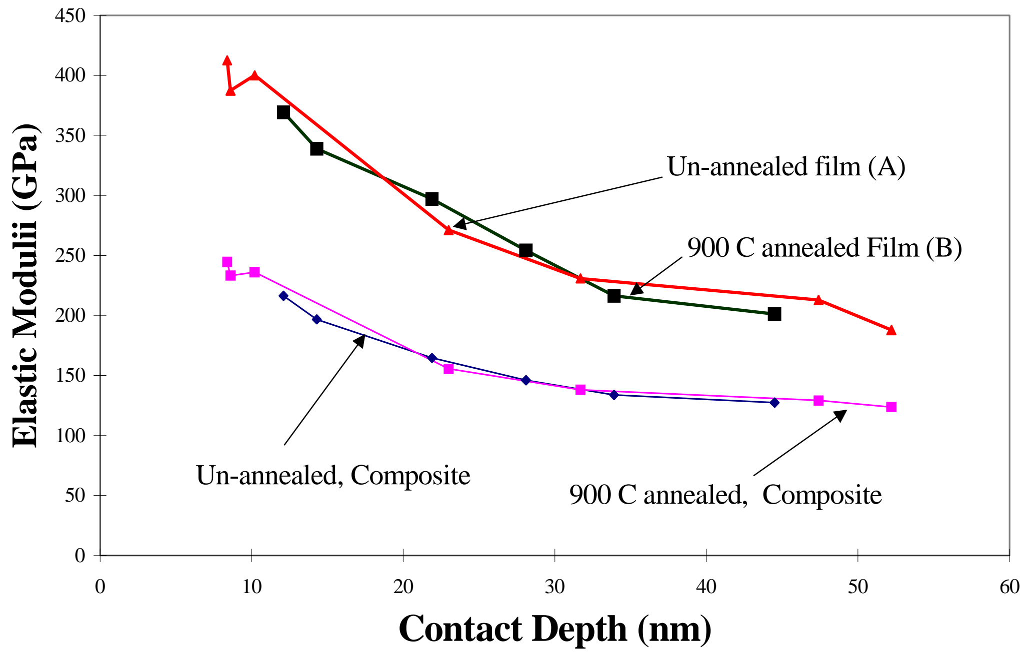

Figure 22: The Modulii of annealed and un-annealed DLC samples

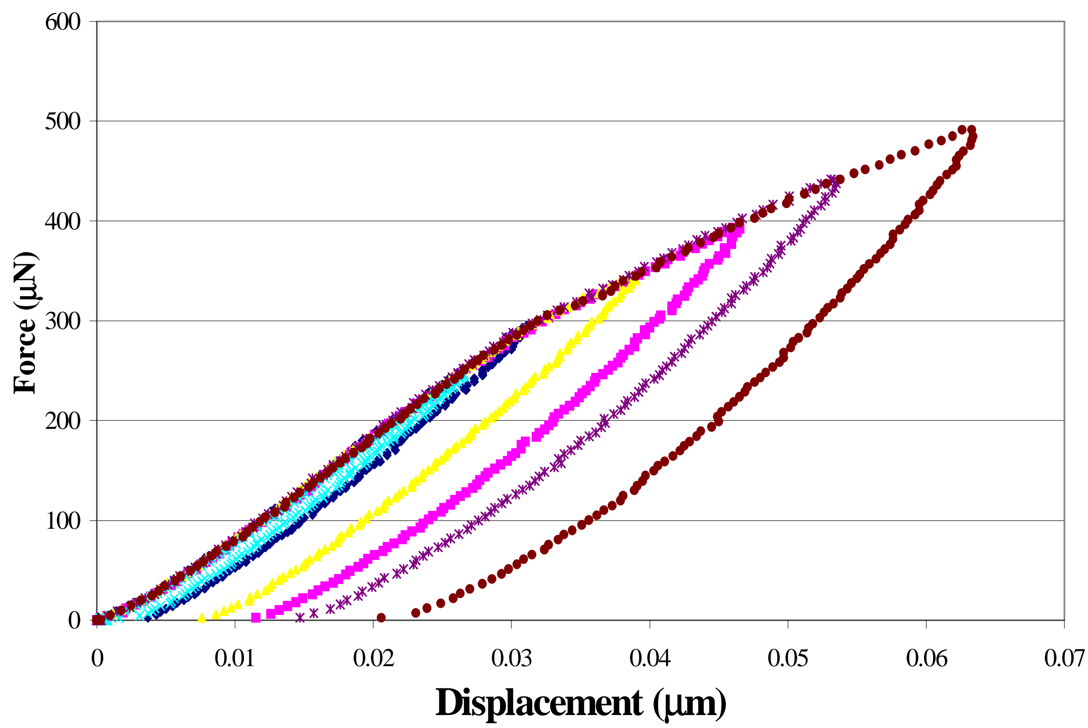

Figure 23: The force/displacement curves for the annealed DLC sample